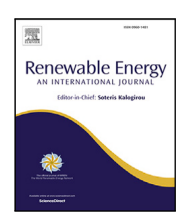
#### Contents lists available at ScienceDirect

### Renewable Energy

journal homepage: www.elsevier.com/locate/renene



## Dynamic analysis of lowering operations during floating offshore wind turbine assembly mating

Can Ma<sup>a</sup>, Taiyu Zhang<sup>a</sup>, Zhiyu Jiang<sup>b</sup>, Zhengru Ren<sup>a,\*</sup>

- a Institute for Ocean Engineering, Shenzhen International Graduate School, Tsinghua University, Tsinghua Campus, University Town, Shenzhen 518055, China
- <sup>b</sup> Department of Engineering Sciences, University of Agder, N-4898 Grimstad, Norway

#### ARTICLE INFO

# Keywords: Floating offshore wind turbines Lowering operation Wind turbine installation Re-impact phenomena Dynamic analysis

#### ABSTRACT

An integrated method for tower–nacelle–rotor assemblies has been proposed as an innovative approach to the transportation and installation of floating offshore wind turbines. This efficient approach offers potential value to the industry with increasing turbine sizes. During the mating phase at an offshore site, the installation system becomes a complex multibody system that involves a vessel, a wind turbine assembly, a crane, and a floating foundation. While much existing research focuses on the steady-state dynamic analysis of the lifted turbine assembly in fixed positions, the lowering operation of the assembly is an unsteady process with potential risks. To this end, this paper develops a fully coupled multibody model for the lowering scenario, accounting for the effects of environmental loads on the overall dynamic responses and the couplings between the multibodies. The study reveals the occurrence of re-impact phenomena between the foundation and the lifted structure under environmental loads, and the backward motion of the installation vessel during lowering. The selection of lowering speed and time instant for starting the operation both influence the occurrence of re-impact. Numerical simulation results offer valuable insights for heavy payload lowering operations and contribute to further decision making of assembly transportation and installation processes.

#### 1. Introduction

To limit global warming to 1.5 °C, the 28th united nations climate change conference requires increasing the renewable energy capacity three-fold by 2030. Offshore wind energy is one of the fastest growing renewable energy. Floating offshore wind turbines (FOWTs) are the potential choice in deep water, i.e., water depth more than 100 m, where the construction costs of traditional bottom-fixed offshore wind turbines (OWT) become prohibitive. However, a high levelized cost of energy still limits the development of FOWTs [1,2]. Two major trends have been observed in the commercial projects. First, upscaled larger OWTs with higher energy harvesting capacity are being applied [3]. Second, an increasing number of turbines are deployed in recent floating offshore wind farms, e.g., Kincardine, Hywind Tampen, and Hainan Wanning. Both trends lead to an urgent need for efficient transport and installation (T&I) methods [4].

Wet-towing is a commonly employed T&I method for the installation of semi-submersible FOWTs. An FOWT is completely assembled onshore and subsequently towed to the installation site using tugboats. However, the slow transportation speed and the need for a long weather window result in costly long-distance towing operations.

Therefore, newly developed T&I methods are demanding to improve the installation efficiency and reduce the whole cost of offshore wind energy utilization. Novel installation methods [5], specialized installation vessels [6-9], and innovative lifting solutions [10,11] provide various options for FOWT T&I. For example, a heavy floating crane vessel, Saipem 7000, was used in the FOWT installation in the Hywind Scotland project. Tower-nacelle-rotor assembly integrated installation method [12] offers an alternative T&I method. The whole process of the FOWT installation using the assembly integrated installation method [13] can be summarized by four steps. (a) loading the assemblies onboard and transporting them to the installation site, (b) activating the dynamic positioning (DP) system at the installation site and connecting to the foundation, (c) decision-making and implementation for the mating operation, and (d) decoupling between the foundation and the vessel and termination of the operation. First, multiple topside assemblies are constructed on land and carried on the vessel deck to the installation site. Increasing the number of assemblies per transport can reduce the overall offshore installation time. It also increases the requirement for vessel capacity. During the positioning and coupling operation, a mechanical gripper or fender [14] is equipped at the stern of the vessel to maintain relative motions in the horizontal

E-mail address: zhengru.ren@sz.tsinghua.edu.cn (Z. Ren).

<sup>\*</sup> Corresponding author.

plane with the moored floating foundation. The DP system counteracts environmental loads [15,16]. After coupling the vessel with the floating foundation, a lifting system on the dock is used to lift one of the assemblies and move it to the stern.

The assembly integrated installation method has been developed recently. A low-height lifting system [17], with a lower crane height, avoids the need for large-scale cranes, further reducing installation costs. Additionally, its associated control scheme [18] is proposed for the growing size and weight of the assembly. Alternatively, a hydraulic active heave compensation system [19] is proposed to minimize the relative positions between the mating points (i.e., the centers of the spar topside and the lifted assembly bottom). A concept of contactless anti-swing control using a magnetic interaction actuator is proposed [20]. The application of actuator offers enhanced possibilities for the design of the novel installation method. Besides, using SWATH vessel [21] as the installation plant is further investigated to evaluate the wave-structures responses.

Fully coupled dynamic analysis facilitates the revelation of possible risks prior to actual operations. The integrated installation system, consisting of a floating vessel, a floating foundation, and a lifted assembly, represents a typical multibody dynamics problem. Conducting steadystate simulations for critical scenarios is the most commonly employed research method to analyze the system dynamics. Steady dynamic response simulations [22,23] have been performed when the assembly is lifted over the foundation. A frequency-domain framework for floating installation of the OWT towers is preliminarily investigated to assess the operability [24,25]. However, steady-state simulations [26] may overestimate the motion responses of multibody systems compared to nonstationary simulations. Moreover, the potential impacts [27] influence the whole responses and other coupling forces. The impact force magnitude is directly influenced by the relative velocity and is sensitive to the sea conditions. Finite element method [28-30] can be used for further verification of the local structural damage.

The lowering operation of a wind turbine assembly is a key step during the mating operation. Numerical modeling and dynamic analysis of dual-body [31-33] and multibody [34,35] lifting schemes have been conducted. The one-time OWT lifting operation is classified as heavy lifting due to the substantial weight of the assemblies, presenting challenges such as crane lifting capacity [36]. The influence of the crane flexibility on the lifting processes has been studied [37,38]. Besides, the elongated shape of the lifted assembly also presents challenges. The implementation of anti-tippling mechanisms is essential to maintain the vertical orientation of the wind turbine tower throughout the mating operation [39]. During the lowering operation, load transfer occurs, resulting in a tilt of the installation vessel. The spar, influenced by the mechanical gripper, similarly tilts in the same direction. Consequently, the DP system must counteract the forces generated by the spar's inclination to maintain stability. Furthermore, the alignment and connection between the assembly and the floating foundation require additional considerations. Essential decision support is indispensable when conducting the lowering operations. Traditional decision-making methods typically involve personnel making decisions based on sea states. In order to ensure the safety of offshore operations, intelligent decision-making methods are continuously being proposed [40-45].

To the best of the author's knowledge, limited existing research addresses the nonstationary dynamic process of the lowering operation. The discontinuous impact loads [46], hydrodynamic interactions [47, 48], and coupling effects during the lowering operation need to be further investigated in the time domain. Time-domain dynamic simulations can reveal potential safety hazards during installation and controller design guidelines at different stages.

This study investigates comprehensive multibody dynamic behaviors during the lowering operation. The main contributions of the paper include the following:

- The impact between the lifted assembly and foundation is modeled. The re-impact and the backward motion of the vessel phenomenas are revealed.
- A discussion on controller gain of the DP system, lifting speed, start time of the winch, and sea states is performed. The influence of these factors on the occurrence of re-impact and backward motion phenomena are revealed.
- Simulations of the lowering operation are conducted under various sea states, followed by a statistical analysis of the coupling forces (e.g., lifting wire, gripper, and contact forces) and motion responses of the installation system.

This paper is organized as follows. In Section 2, the concept of the installation system and the challenges are described. Section 3 introduces the modeling details of the installation system, with a focus on the mating operation. In Section 4, simulations for the lowering operation are conducted in calm waters and different sea states. Additionally, the control effectiveness of the DP system, and the influence of winch speed and sea state are discussed. Finally, conclusions are summarized in Section 5.

#### 2. System description

The complete T&I process of the tower–nacelle–rotor assembly integrated installation method is illustrated in Fig. 1.

#### 2.1. Description of the installation system

The research scenario comprises four major components: a catamaran, a moored floating foundation, a crane, and multiple OWT assemblies. The catamaran is used as the installation vessel to transport the assemblies and serves as the platform for the mating operation. The crane and devices for securing the assemblies are rigidly fixed on the deck. One of the OWT assemblies is lifted to the stern of the vessel, awaiting the mating operation after the installation vessel is connected to the floating foundation. For clarity, the OWT assembly awaiting release is referred to as the payload in the following context.

In Step (a), the floating foundation without superstructure can be moored in advance, allowing large-scale assemblies to be transported directly to the installation site. This approach simplifies both the transportation and installation processes, streamlining the construction of large-scale wind farms. The installation vessel is equipped with a DP system to counteract wind, currents, and second-order wave loads. Additionally, the vessel is fitted with mechanical grippers to maintain its relative position to the foundation. Passive rollers are integrated at the edges of the grippers, exerting no constraints on the vertical motion of the spar foundation. In Step (b), a temporary weak coupling is established using the mechanical gripper to ensure stable horizontal positioning between the installation vessel and the floating foundation. Anti-toppling devices for the lifting operation, such as traction wires and mechanical stabilizers, are also incorporated into the system.

#### 2.2. Description of the lowering operation

In Step (c), the lowering operation is crucial in the tower–nacellerotor integrated lifting method. During the lowering operation, the crane gradually releases the lifting wires to lower the payload, without crane movement. The mechanical anti-tippling device maintains the payload vertically. After the payload contacts the spar foundation, the transfer of its weight from the installation vessel to the spar foundation results in a draft change for both structures. Due to the large waterline area of the installation vessel, the draft change is less pronounced during load transfers. After completing the mating operation, the installation vessel disconnects the mechanical coupling from the spar foundation and deactivates the DP system. In Step (d), ballast water management can be used to adjust the state of the installation vessel, allowing it to move towards the next site.

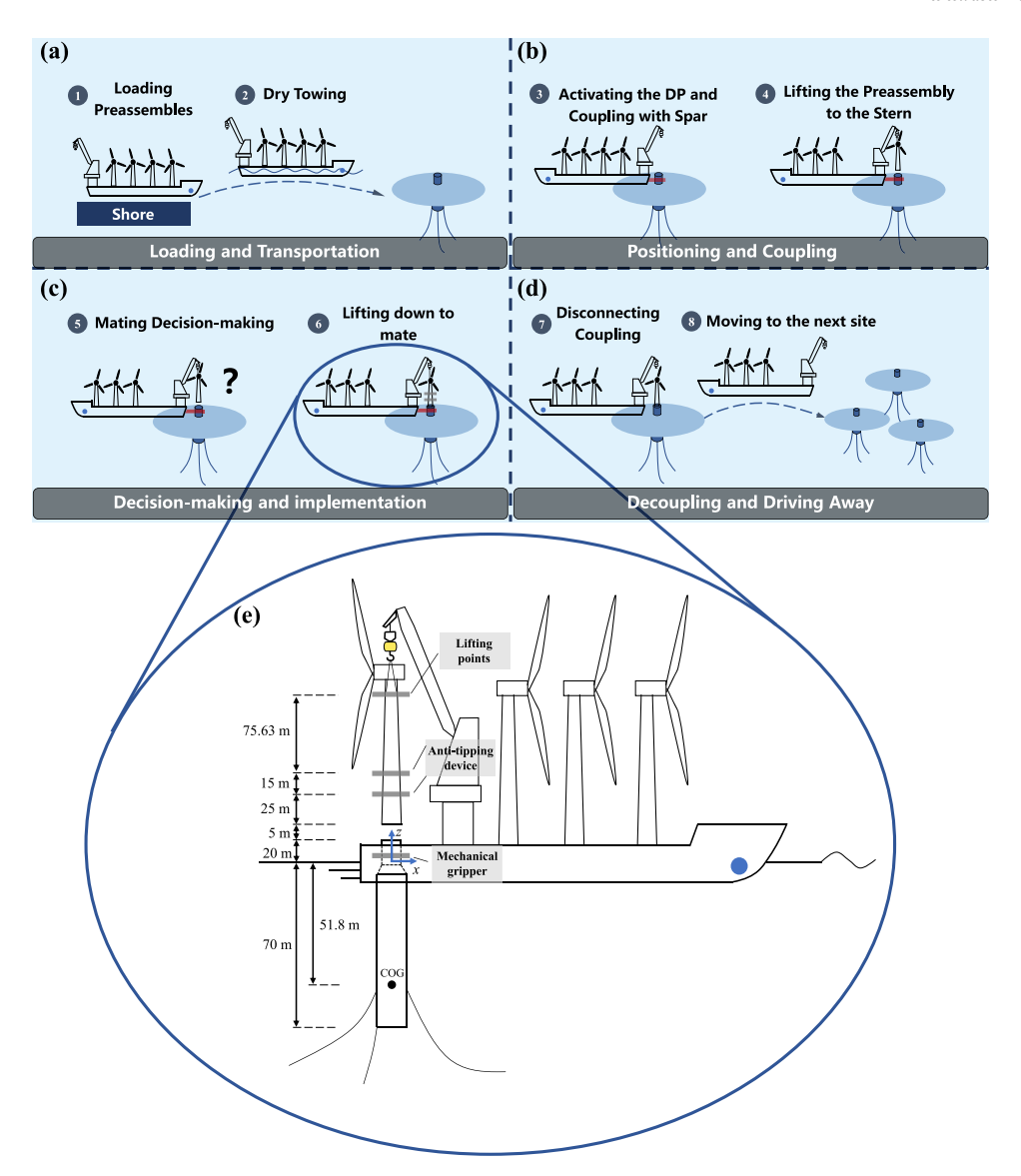


Fig. 1. (a)-(d): Steps of the T&I process; (e): Set up of the installation system.

Since the installation vessel and the spar foundation are not completely rigidly coupled, relative motions occur under environmental loads. The mechanical grippers help prevent direct impacts between the vessel and the spar foundation. However, suspending the heavy payload with wires from the vessel presents a significant risk of impact due to relative vertical motions, particularly the relative pitch motion between the vessel and the spar foundation. While increasing the displacement of the installation vessel can enhance stability, it is essential to analyze the relative motion between key mating points during the lowering operation.

#### 3. System modeling

The system is modeled using SIMA, enabling time-domain simulations of multibody systems in marine operations. The main components of the installation system are modeled as rigid bodies. Each body is connected through coupling modules with others, as shown in Fig. 2. Apart from the lifted assembly, the remaining assemblies on the deck are rigidly fixed, with consideration of their impact on the hydrodynamic parameters of the installation vessel. The crane is simplified as a lifting system, where a winch at the top of the lifting wire replaces the rigidly connected crane on the installation vessel. The main parameters of the spar foundation, the catamaran vessel carrying

three wind turbine assemblies, and the lifted assembly are illustrated in Table 1. The parameters of the catamaran are calculated by reflecting the mass distribution with three rigidly connected assemblies. While the parameters of the spar foundation are calculated with no ballast and the upper turbine superstructure.

A global coordinate system is defined following the right-hand rule, with the origin positioned at the axial center of the horizontal plane of the spar. The *x*-axis points towards the North, the *y*-axis is towards the West, and the *z*-axis is set upwards. All responses of the bodies provided below are expressed in the global coordinate system. The motions of the spar topside center can be calculated using coordinate transformation.

#### 3.1. Hydrodynamic loads

Added mass and potential damping are calculated in the frequency domain, and then applied in the time domain for the coupled motion analysis of the two bodies using retardation functions. The hydrodynamic interaction between the vessel and the spar is also considered [39]. The viscous forces on the installation vessel are represented by linear roll damping and quadratic yaw damping coefficients.

The additional viscous drag forces acting on the spar foundation should be accounted for. The viscous drag forces per unit length is expressed by the Morison drag equation,

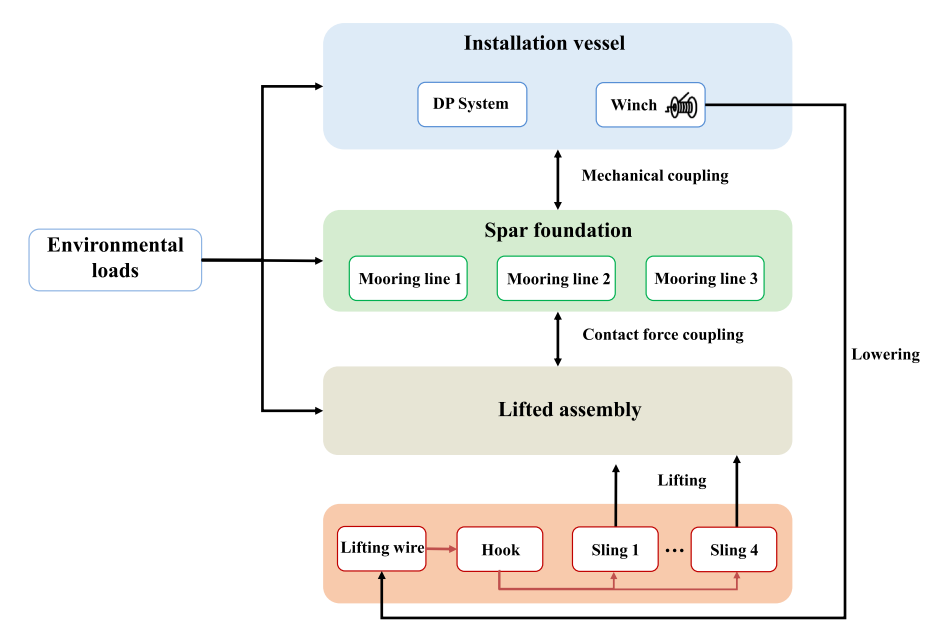


Fig. 2. Modeling framework.

Table 1
Parameters of the installation system.

Parameters	Unit	Value		
Catamaran with assemblies				
Length	m	144		
Width	m	60		
Spacing between mono-hulls at waterline	m	38		
Draft	m	8		
Displacement mass	tonnes	18 503		
Vertical position of COG	m	28.6		
Transverse metacentric height	m	66.4		
Initial position of reference point	m	(64,0,0)		
Spar				
Diameter at top	m	9.5		
Diameter at waterline	m	14		
Draft	m	70		
Displacement mass	tonnes	11 045		
Vertical position of center of buoyancy	m	-35		
Vertical position of COG	m	-51.8		
Initial position of reference point	m	(0,0,0)		
Lifted assembly				
Rated power	MW	10		
Rotor diameter	m	178.3		
Hub diameter	m	5.6		
Hub height	m	119		
Rotor mass	tonnes	228		
Nacelle mass	tonnes	446		
Tower mass	tonnes	628		
Initial position of the reference point	m	(0,0,25)		

$$df_{drag} = \frac{1}{2} \rho C_d D(u_w - u_i) |u_w - u_i| dz, \tag{1}$$

where  $\rho$  is the density of sea water,  $C_d$  is the drag coefficient, D is the diameter of each spar foundation strip,  $u_w$  and  $u_i$  are the velocities of the water particle and the corresponding discrete element, respectively. In the present paper,  $C_d=0.9$ .

Fig. 3 shows the surge, heave, and pitch force response amplitude operators (RAOs) of the spar foundation and the vessel.

#### 3.2. Aerodynamic forces

The influence of wind loads during the offshore mating operation cannot be ignored, especially for the lifting operation. The aerodynamic forces acting on both the lifted assembly and the assemblies on board are taken into account.

The wind field is assumed to be 2-dimensional, parallel to the horizontal plane, and the wind velocity variation in the mean direction described by the NPD wind spectrum

$$S(f) = \frac{320 \cdot \left(\frac{U_0}{10}\right)^2 \cdot \left(\frac{z}{10}\right)^{0.45}}{(1 + f_m^n)^{5/(3n)}},\tag{2a}$$

$$f_m = 172 \cdot f \cdot \left(\frac{z}{10}\right)^{2/3} \cdot \left(\frac{U_0}{10}\right)^{-0.75},$$
 (2b)

where S(f) is the spectral density, z is the height above sea level,  $U_0$  is the 1 h mean wind speed at 10 m above sea level, and n=0.468 is selected. The wind profile model is adopted to describe the wind speed variation along the height,

$$\bar{u}(z) = \bar{u}_r (\frac{z}{z_r})^{\alpha},\tag{3}$$

where  $z_r=10$  m is the reference height,  $\bar{u}_r$  is the average velocity at the reference height,  $\alpha=0.11$  is the height coefficient, and  $\bar{u}(z)$  is the average velocity at height z. The wind forces are calculated based on the instantaneous relative wind velocities between the wind and body, as well as the fluid interference between different OWT assemblies, is neglected. The force is calculated by

$$q_i = C_i(\alpha) u_{rel}^2, \tag{4}$$

where  $q_i$  is the wind force in ith degree of freedom,  $u_{rel}$  is the instantaneous relative wind speed,  $C_i(\alpha)$  is the wind force coefficient for the instantaneous relative direction, and blades are set to face the incoming wind along the positive direction of the x-axis to calculate the wind force coefficient. Besides, the wind-induced loads on the towers are also considered. The aerodynamics coefficients of the blades are calculated by HAWC2 [12]. Fig. 4 presents variations of the force and moment coefficients acting on a single wind turbine with respect to the main wind direction.

#### 3.3. Lifting system

Model simplification is needed to understand the system dynamics. Differing from the gripper and low-height cranes mentioned in early research, the lifted assembly's suspension points are higher. Factors

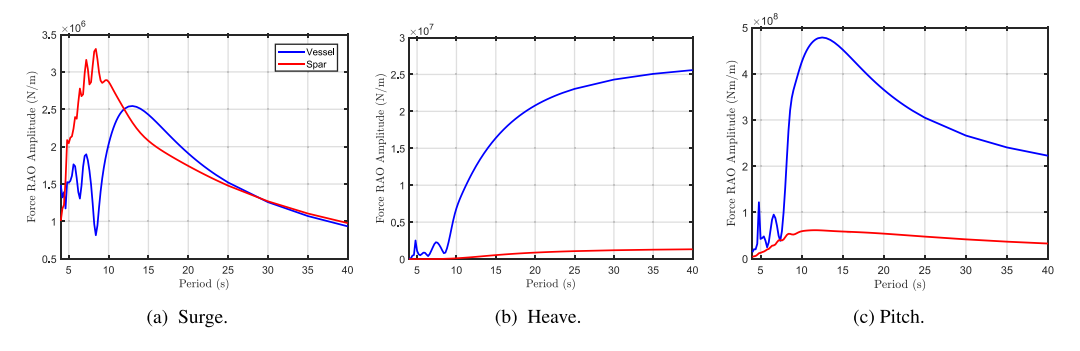


Fig. 3. Selected RAO amplitudes of the free-floating bodies with hydrodynamic interaction.

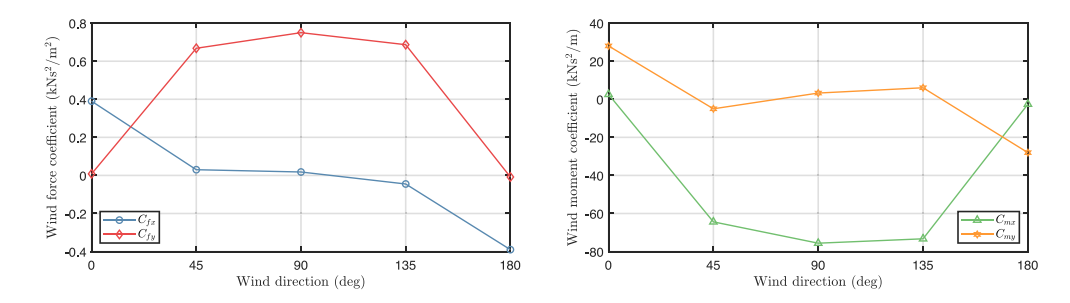


Fig. 4. Wind force and moment coefficients of a single wind turbine.

such as the position of the suspension point and the length of the lifting wire influence the dynamic characteristics [49,50] (e.g., axial rotation of the payload), but they are not analyzed in this study. The model considers the lifting wire that connects the crane tip to the hook, with a winch adjusting the lifting wire length. The hook is modeled as a lumped mass, which is constrained to three translational DOFs. Four slings are split off from the hook to lift the assembly. Consequently, the lifting wire length varies with the winch activity, while the length of the slings remains constant.

The simplified lifting system is illustrated in Fig. 5. The lifting wire and four slings are modeled as linear springs, and the modeling of the lifting wire can take into account the influence of crane flexibility on tension using an overall stiffness

$$\Delta l = \frac{T}{k},\tag{5a}$$

$$\frac{1}{k} = \frac{1}{EA} + \frac{1}{k_0},\tag{5b}$$

where  $\Delta l$  is the elongation, T is the wire tension, k is the effective axial stiffness, E represents the modulus of elasticity, A is the cross-section area, and  $k_0$  represents the connection flexibility providing insight into the crane's structural flexibility. Material damping is typically set at 1%-2% of EA.

To ensure the lifting operation safety and prevent the assembly from tilting, anti-tippling measures must be taken into consideration. The docking cone module is used to model anti-tippling device. The docking cone coupling is simulated as a guide pin attached to the middle of the lifted assembly and a docking cone fixed on the installation vessel. When the guide pin moves horizontally away from the required vertical axis, the anti-tippling device exerts a restoring force pushing the lifted assembly back into position. Two docking cone modules are set vertically along the assembly to maintain the upright position of the assembly and prevent the assembly from rotating in pitch and roll, which may occur if only one docking cone is used. The pin points of the two docking cone modules are located 25 m and 40 m above the bottom surface of the lifted assembly, respectively. The principle of the docking cone and the specific distance-force relationship of the anti-tippling device are shown in Fig. 6.

**Table 2**Parameters of the bumper group.

Parameters	Value	Unit
Number	8 (lower side)	-
	8 (upper side)	
Radius	0.25	m
Length	8.3	m
Stiffness	1e+07	N/m
Damping	1200	Ns/m
Z-coordinate position	20 m (lower side)	m
	25 m (upper side)	

#### 3.4. Contact force

To obtain the overall responses of the installation system, the contact force between the payload and spar foundation is simulated by integrating coupling modules, shown in Fig. 7.

Sixteen slender bumpers are distributed at the bottom of the payload and on topside of the spar, the parameters of the bumpers are shown in Table 2. The contact force between the bumpers is defined through a specified distance-force relation. The stiffness of the bumper group is set sufficiently large to ensure no intersection occurs between the tower and the spar foundation. A small amount of damping is selected to enhance numerical stability, with negligible impact on the system's motions. Moreover, if energy dissipation after impact is to be considered, further refinement of damping maybe necessary.

Since the spar is modeled as a rigid body, the motions of one point on the spar can be known by a coordinate transformation based on the relative position  $I^b$  between the body coordinate origin motion  $p^n_o$  and the point. The OWT body coordinate origin is set at the bottom center of the lifted assembly and it can directly react to the mating point motions.

#### 3.5. Station-keeping system

The station-keeping systems, including the mooring system for the floating foundation and DP system for the vessel, are crucial for maintaining the multibody system in the present scenario. For the spar, three

Fig. 5. Lifting system modeling.

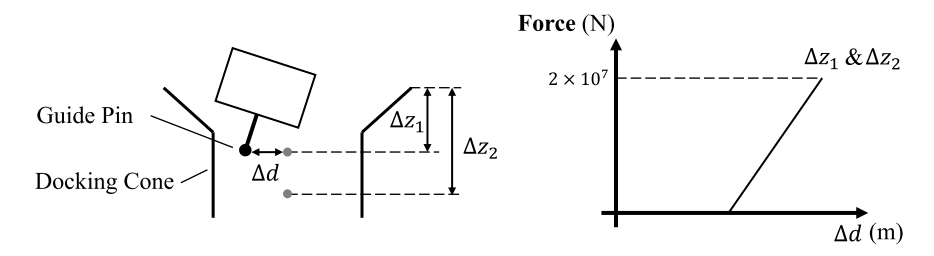


Fig. 6. Mechanical property of the anti-tippling device.

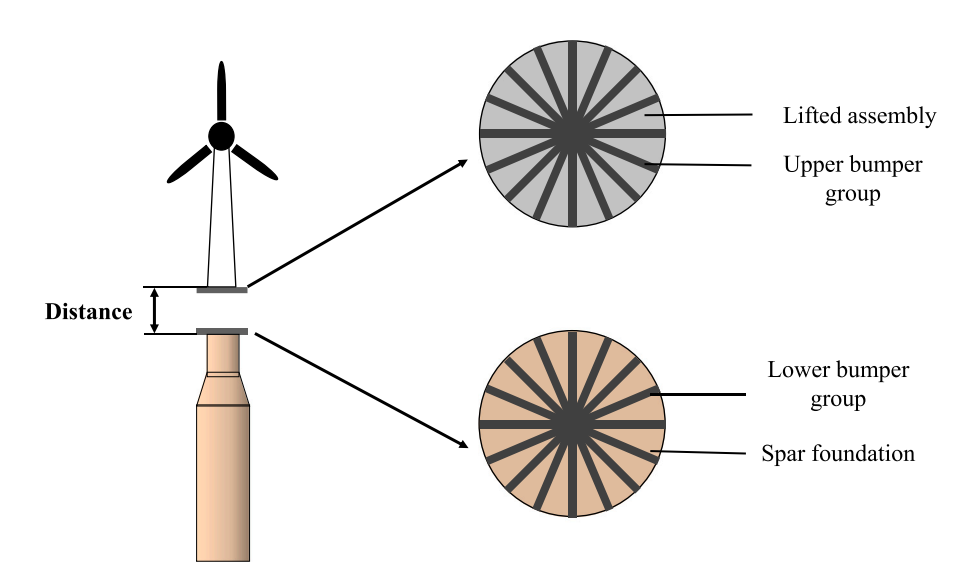


Fig. 7. Modeling of contact force.

catenary lines are distributed with an interval of  $120^\circ$  in the horizontal plane. One of the catenary lines is oriented in the positive direction of the x-axis. Quasi-static analysis and a simplified frequency-domain method are combined for the dynamic tension calculation.

The DP system is important for maintaining the relative motions between the spar and the vessel under hydrodynamic and mechanical loads. The DP system consists of four lateral thrusters and two longitudinal thrusters. The control gains are tuned to an optimal state to ensure successful mating operations. The coupling effects between the spar foundation and the vessel induce a certain degree of motion. It is interesting to follow up with an investigation of DP system performance on installation.

#### 3.6. Equations of motion

The equations of motion for the multibody system can be expressed as

$$(M+A(\infty))\ddot{\mathfrak{x}}+D_1\dot{\mathfrak{x}}+D_2f(\dot{\mathfrak{x}})+K(\mathfrak{x})\mathfrak{x}+\int_0^th(t-\tau)\dot{\mathfrak{x}}(\tau)d\tau=q(t,\mathfrak{x},\dot{\mathfrak{x}}), \quad (6)$$

where M is the mass matrix,  $A(\cdot)$  is the frequency-dependent added mass matrix,  $D_1$  and  $D_2$  represent linear and quadratic damping matrices,  $f(\cdot)$  represent the vector function where each element is given by  $f=\dot{\mathfrak{x}}|\dot{\mathfrak{x}}|$ .  $K(\mathfrak{x})$  is the hydrostatic stiffness,  $\mathfrak{x}$  denotes the position vector of the rigid body, h is the retardation function computed by a transform of the frequency-dependent added-mass and damping, and q

Table 3
Parameters to be considered.

	DP system	Winch speed	Start instant of the winch	Sea state
Section 4.2 (calm water)	Different control gains	Fixed	Fixed	NA
Section 4.3 (environmental loads)	Fixed	Different speed	Different lowering instant	Different $H_s$ , $T_p$

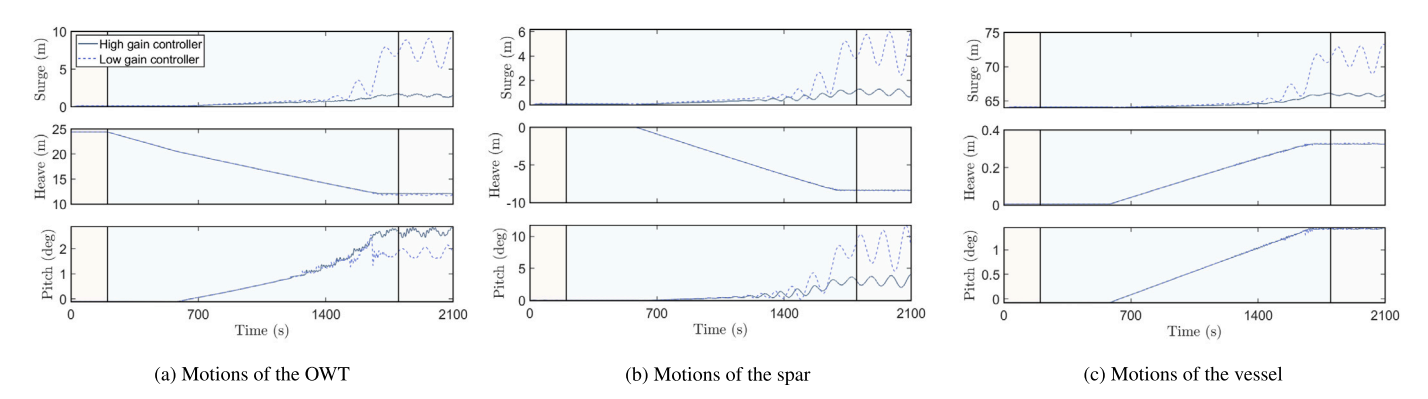


Fig. 8. Motion behaviors in the calm water using DP systems with different control gains.

is the exciting force which includes the wave loads, wind loads, and other loads.

#### 4. Results and discussion

#### 4.1. Simulation overview

To investigate the performance of the lowering operation in different sea states and lifting sets, the selected parameters are listed in Table 3. A simulation in calm waters is used to reveal the dynamics of the lowering operation and verify the modeling fidelity. The impact of high gains and low gains in the DP system is considered, and the parameters are listed in Table 4. The maximum thrust of the propeller remains unchanged, with only the control parameters in the surge direction being modified.

Subsequently, the lowering operation is simulated under environmental loads, considering different winch speeds and sea states. Irregular wave loads are generated by the Jonswap spectrum. The directions of wave and wind loads are both aligned with the *x*-axis. The simulations last for 2100 s. Based on static calculations, the complete transfer of the payload weight to the spar results in an 8.4 m increase in the spar's draft. The duration of the lowering process is influenced by the lowering speed.

#### 4.2. Dynamic responses in calm water

Lowering operations in the hydrostatic environment can evaluate system dynamics and validate the modeling. At 200 s, the winch begins to lower the payload at a rate of 0.01 m/s and ceases lowering operation at 1800 s. Fig. 8 illustrates the motion characteristics during the lowering operation, which can be divided into three distinct phases, i.e., pre-lowering, lowering, and landing. Only three DOFs are plotted to illustrate the dynamic responses, since the surge, heave, and pitch motions are the most important DOFs. The solid line and dotted line represent the system responses with DP controller of higher gains and lower gains, respectively. Both DP systems manage to stabilize the vessel before the lowing operation.

Fig. 8(a) shows the motions of the payload. Due to the constraint imposed by the anti-tipping device rigidly attached to the vessel, the surge and pitch responses of the payload and vessel are similar. Figs. 8(b) and 8(c) present the responses of the installation vessel and spar with different controller gains in the DP system in calm water. As the

Table 4
DP control system parameters.

	Controlled DOF	Proportional (N/m)	Derivative (Ns/m)
High-gain DP	Surge	39 478	8.8e+05
Low-gain DP	Surge	1.97e+05	4.4e+06

payload firstly contacts with the spar at approximately 600 s and is subsequently lowered, its weight is gradually transferred to the spar. The installation vessel experiences smaller changes in draft compared to the spar, attributed to its displacement. The gradual transfer of the payload's weight induces a slow rotational tilt of the vessel around the positive *y*-axis. The mechanical coupling force between the spar and installation vessel induces tilting of the spar and a backward motion of the vessel. To the best of the authors' knowledge, the phenomenon has not been reported. Furthermore, the translational positions and pitch angles of the spar influence the vessel's responses, indicating the substantial stiffness of the mechanical gripper between the vessel and the spar.

DP system influences the translational motions of the whole system. Higher control gains can effectively limit the backward motion of the installation vessel during the lowering operation. Under the influence of a more effective DP system, the vessel demonstrates minimal translational drift in the surge direction of 2.14 m. In contrast, a less effective DP system results in a significantly greater translational drift of 9.3 m, influencing the execution of the lowering operation.

Fig. 9 presents the time-domain results of the mooring lines tensions, the mechanical gripper constraint forces, the anti-tipping forces, the lifting wire tensions, and the bumper impact forces. In the figure, unlabeled forces indicate the magnitude of the vectorial forces. The gripper and anti-tipping forces are influenced by the backward motion and the performance of the DP system, whereas the forces on the lifting wire and the total bumper impact forces are closely related to the vertical weight and remain unaffected. Compared to the DP controller with low gains, the amplitude and oscillation of the gripper and anti-tipping forces are reduced when using the DP controller with higher gains. The capacity of the thrusters and the gains of the DP controller are pre-

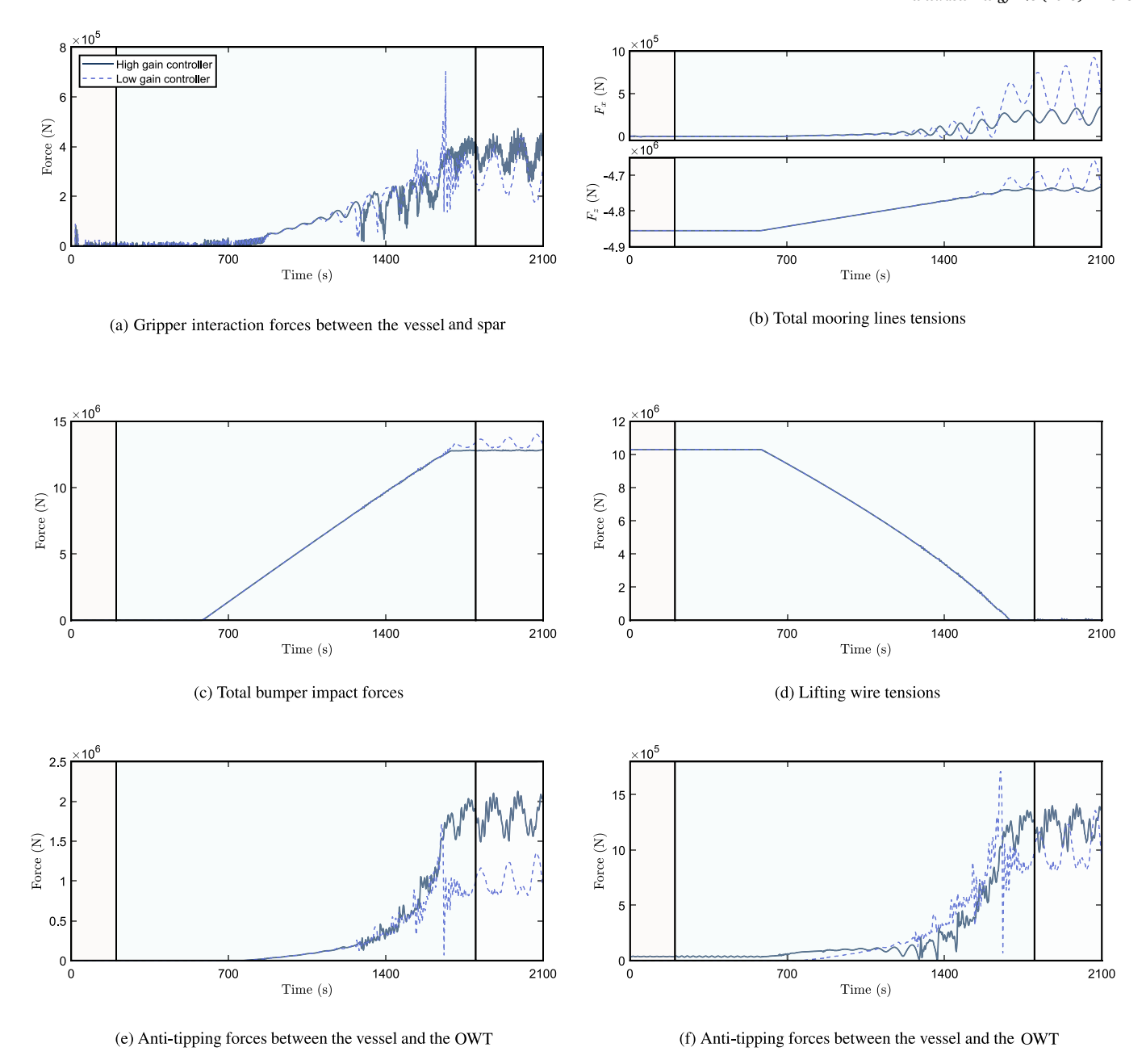


Fig. 9. Coupling forces in the hydrostatic environment using DP systems with different control gains.

Table 5
Winch setting in the simulations.

	Lowering speeds $v_l$ (m/s)	Start time of winch (s)	End time of winch (s)	Lowering length of lifting wire $v_l \times t$ (m)
WS1	0.01	200	1800	16
WS2	0.02	200	1000	16
WS3	0.05	200	520	16
WS4	0.1	200	360	16
WS5	0.1	250	410	16
WS6	0.1	300	460	16
WS7	0.1	350	510	16

determined and limited by design. To counteract the backward motion induced by the lowering operation, the DP controller's additional gains or thruster capacities require further consideration.

To sum up, the backward motion of the installation vessel during the lowering operation results from load transfer and multi-body

coupling forces. Increasing the DP control gains can effectively reduce the motion amplitude, enhancing safety and efficiency. However, due to constraints on propeller thrust and lifespan, the DP gains cannot be increased indefinitely, making it essential to address the limitation during the operational design phase.

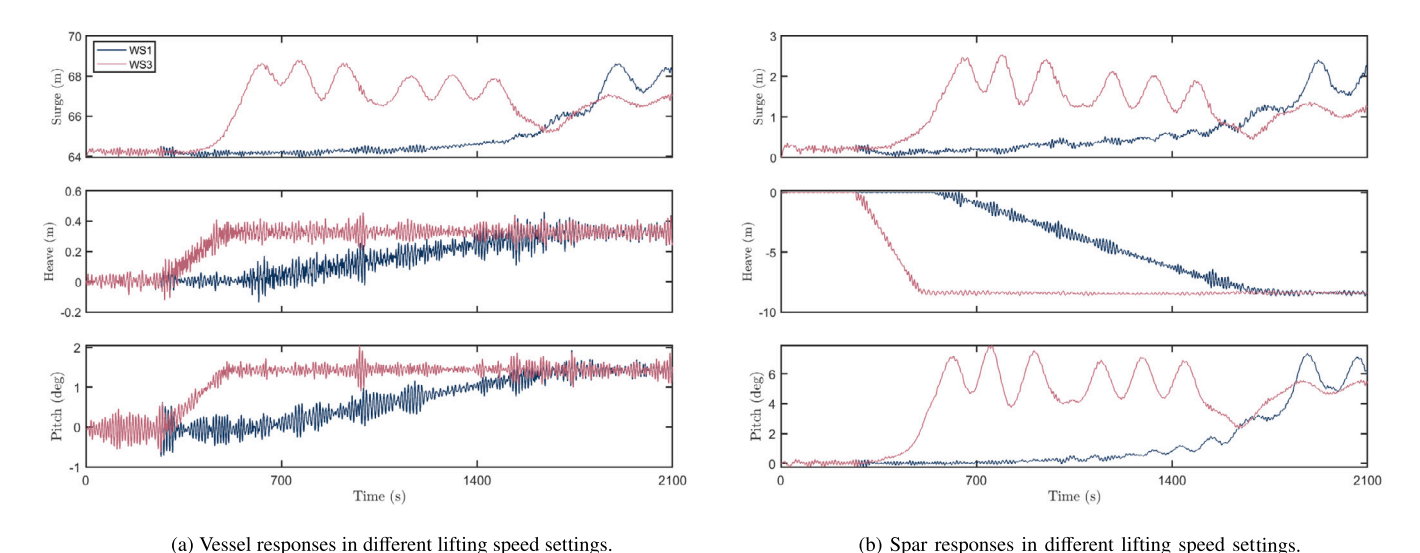


Fig. 10. Dynamic responses in WS1 and WS3.

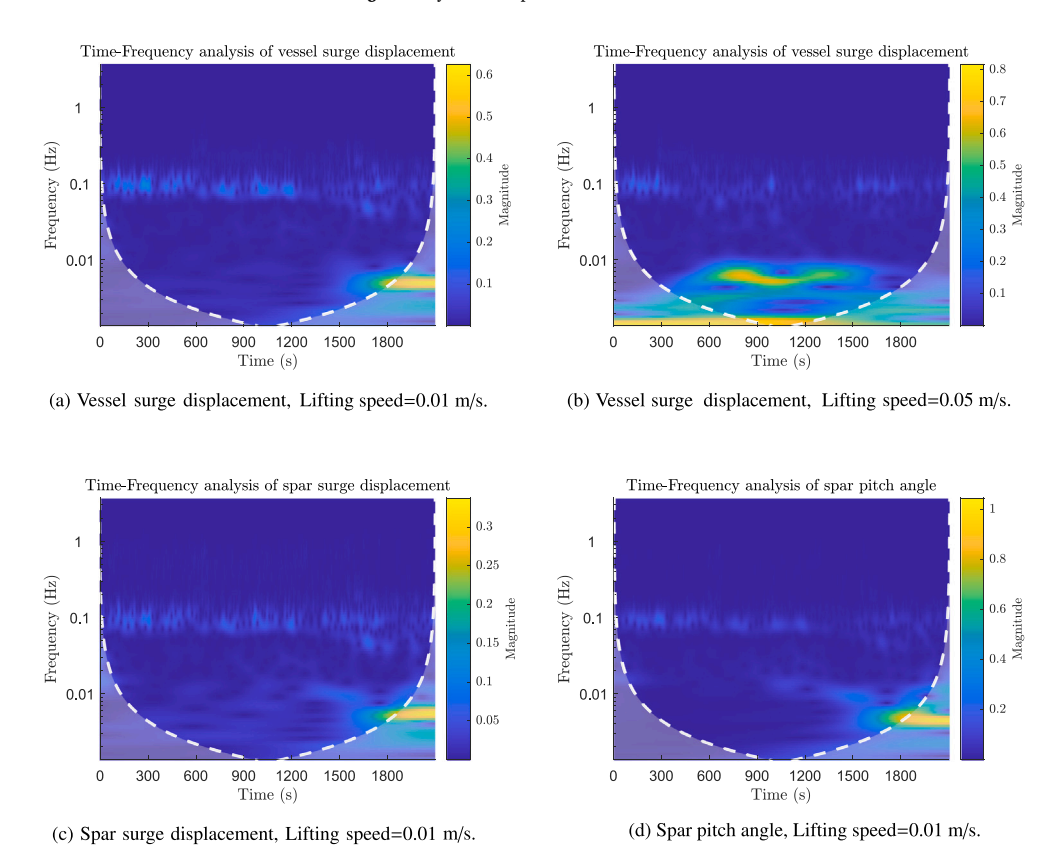


Fig. 11. Time-frequency analysis of dynamic responses in WS1 and WS3.

#### 4.3. Motion behavior under different lifting settings in a selected sea state

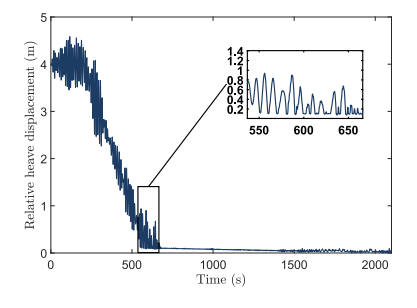
An analysis of the dynamic response of the system under different winch speeds is conducted with  $H_s=0.5~\mathrm{m}$ ,  $T_p=10~\mathrm{s}$ , and the highgain DP control system. Setting different lowering speeds  $v_l$  for the winch, the lowering length of the lifting wire  $v_l \times t$  remains constant. The parameters of the winch setting are shown in the Table 5.

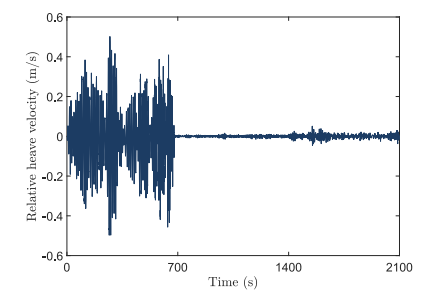
Fig. 10 illustrates the responses of the vessel and the spar in WS1 and WS3. The results indicate that the motions of the installation vessel and the spar are similar in a hydrostatic environment. However, both exhibit irregular fluctuations under the influence of environmental

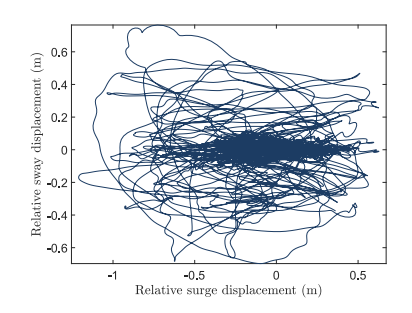
loads. Additionally, the velocity of the winch impacts the rate of response variations, with higher speeds leading to quicker changes in the overall responses and earlier contact between the OWT and spar. Time-frequency analysis of the system's dynamic responses is performed based on wavelet transform, as shown in Fig. 11. Besides the motion responses induced by the wave peak period  $T_p$ , the lowering operation induces low-frequency components in the vessel's surge motion, as well as in the spar's surge and pitch motions. To avoid redundancy, time–frequency analysis is conducted only in WS1 in the following.

Due to the lack of constraints between the OWT and the spar, separation and re-impact occur between them under wave loads when operations are conducted without external interference.

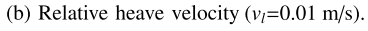
C. Ma et al. Renewable Energy 243 (2025) 122528



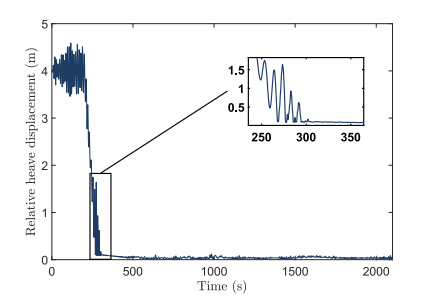


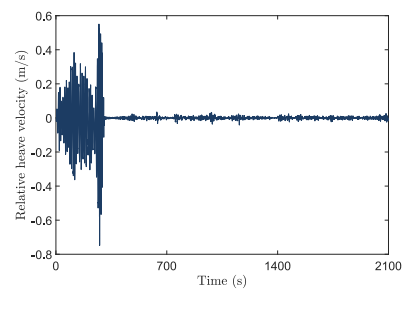


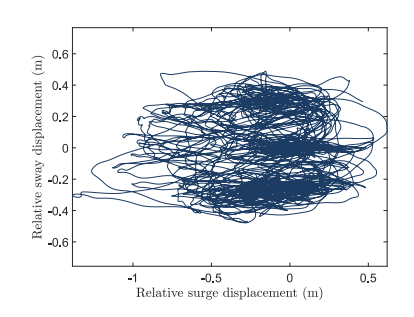
(a) Relative heave displacement ( $v_l$ =0.01 m/s).



(c) Relative motion in the horizontal plane ( $v_l$ =0.01 m/s).





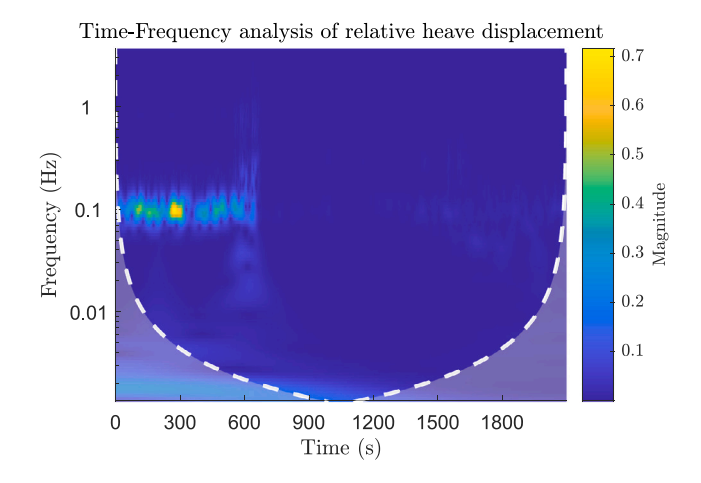


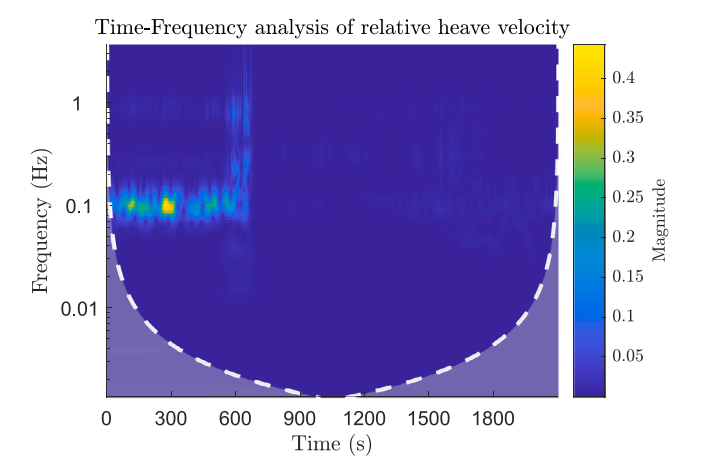
(d) Relative heave displacement ( $v_l$ =0.05 m/s).

(e) Relative heave velocity ( $v_l$ =0.05 m/s).

(f) Relative motion in the horizontal plane ( $v_l$ =0.05 m/s).

Fig. 12. Relative motions between the mating points in WS1 and WS3.





(a) Relative heave displacement, Lifting speed=0.01 m/s.

(b) Relative heave velocity, Lifting speed=0.01 m/s.

Fig. 13. Time-frequency analysis of relative heave motions in WS1.

Table 6
Simulation results under different winch settings.

	WS1	WS2	WS3	WS4	WS5	WS6	WS7
First impact time after start (s)	560.5	382.9	268.4	237.7	288	341.9	390.6
End time of the re-impact after start (s)	677.7	432.7	301.9	244.5	306.1	350.6	399.7
Duration of re-impact (s)	117.2	49.8	33.5	6.8	18.1	8.7	9.1
Lifting wire deployment length at the time of first impact (m)	3.605	3.658	3.42	3.77	3.8	4	4.1
Maximum relative heave displacement after impact (m)	1.29	0.979	2.026	0.589	1.29	0.548	0.587
Maximum relative surge displacement (m)	1.21	1.78	1.38	1.36	1.71	1.99	1.38
Maximum relative sway displacement (m)	0.76	0.55	0.49	0.66	0.42	0.51	0.41

Fig. 12 shows the relative motions between the mating points in WS1 and WS3. Re-impacts occur before the weight of the OWT is fully

transferred. The magnitude of the relative displacement along the z-axis post-impact is 1.5 m at a lifting speed of 0.05 m/s, which is larger

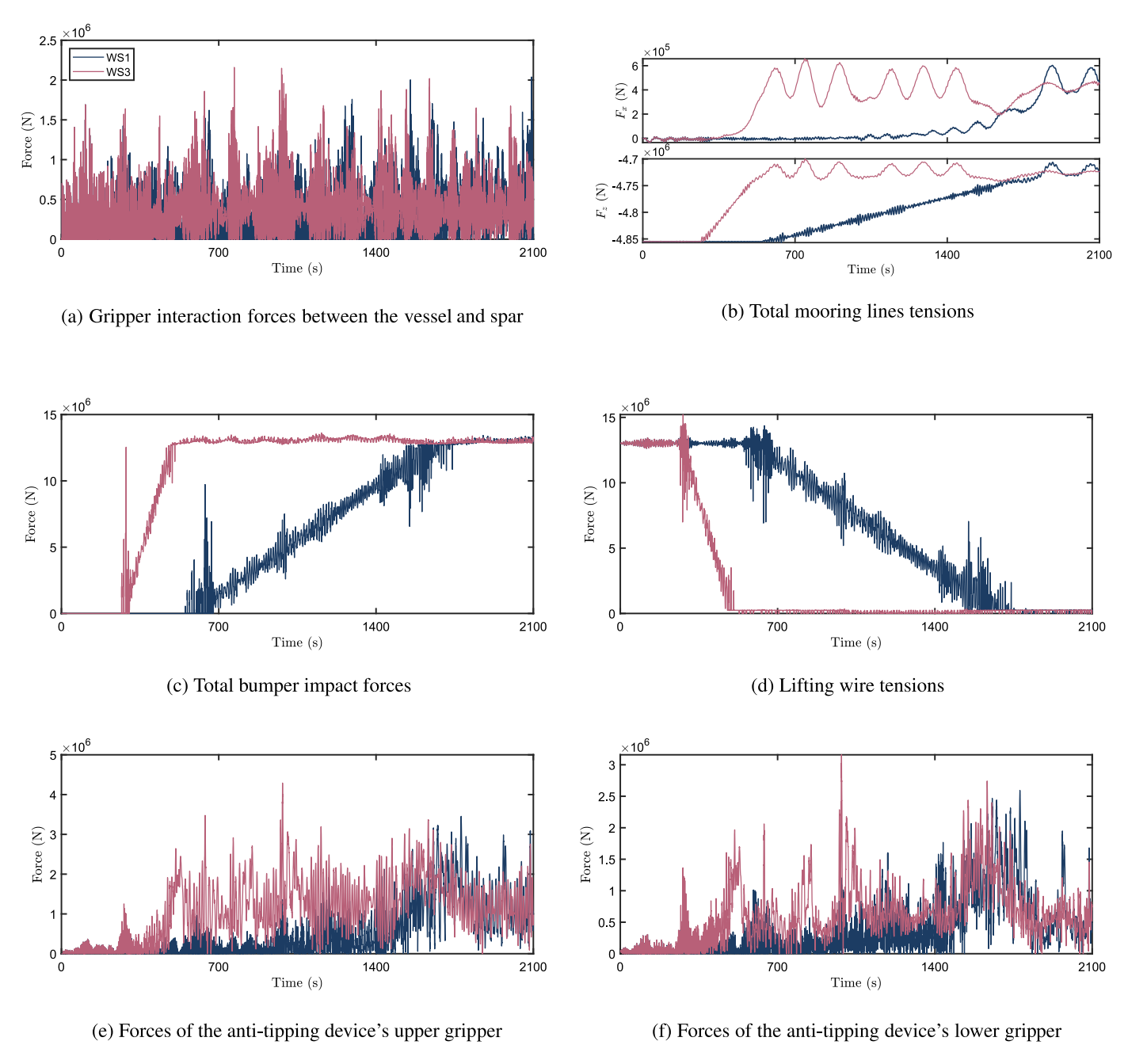


Fig. 14. Coupling forces in WS1 and WS3.

than the magnitude of 0.8 m at a lifting speed of 0.01 m/s. After the re-impact phase, the relative heave displacement stabilizes. The time–frequency analysis of the relative motions is shown in Fig. 13. During the re-impact phase, high-frequency relative heave motions are observed. In the horizontal plane, a greater relative displacement along the x-axis at the lifting speed of 0.05 m/s while reducing relative displacement along the y-axis. The re-impact phase has a negative effect on the mating operations, such as tightening bolts.

The main simulation results regarding winch speed and start time are summarized in the Table 6. The first contact between OWT and spar occurs at 560.5 s, 382.9 s, 268.4 s, 237.7 s, 288 s, 341.9 s, 390.6 s for each respective condition, respectively. After the winch has deployed a lifting wire longer than 3.4 m, there is a potential for the bottom of the OWT to impact with the spar. As the winch speed increases,

the duration of re-impacts decreases. Additionally, due to the transient effects of nonlinear wave loads, the timing of contact between the OWT and the spar is a critical factor influencing the amplitude of the post-impact. Wave sensing and motion prediction are effective strategies for preemptively controlling re-impact responses.

Fig. 14 shows the corresponding coupling forces for WS1 and WS3. Due to varying winch speeds, the payload contacts the spar at different time instants, resulting in sudden changes in the amplification of forces on the lifting wire, mooring lines, and bumper. In WS3, it is observed that the impact between the OWT and the spar generates more significant bumper impact loads, resulting in a larger abrupt change in lifting wire dynamic tension. The amplitude of the bumper is closely associated with the relative velocity at the instant of impact. The relative velocity is determined by the stern velocity caused by

C. Ma et al. Renewable Energy 243 (2025) 122528

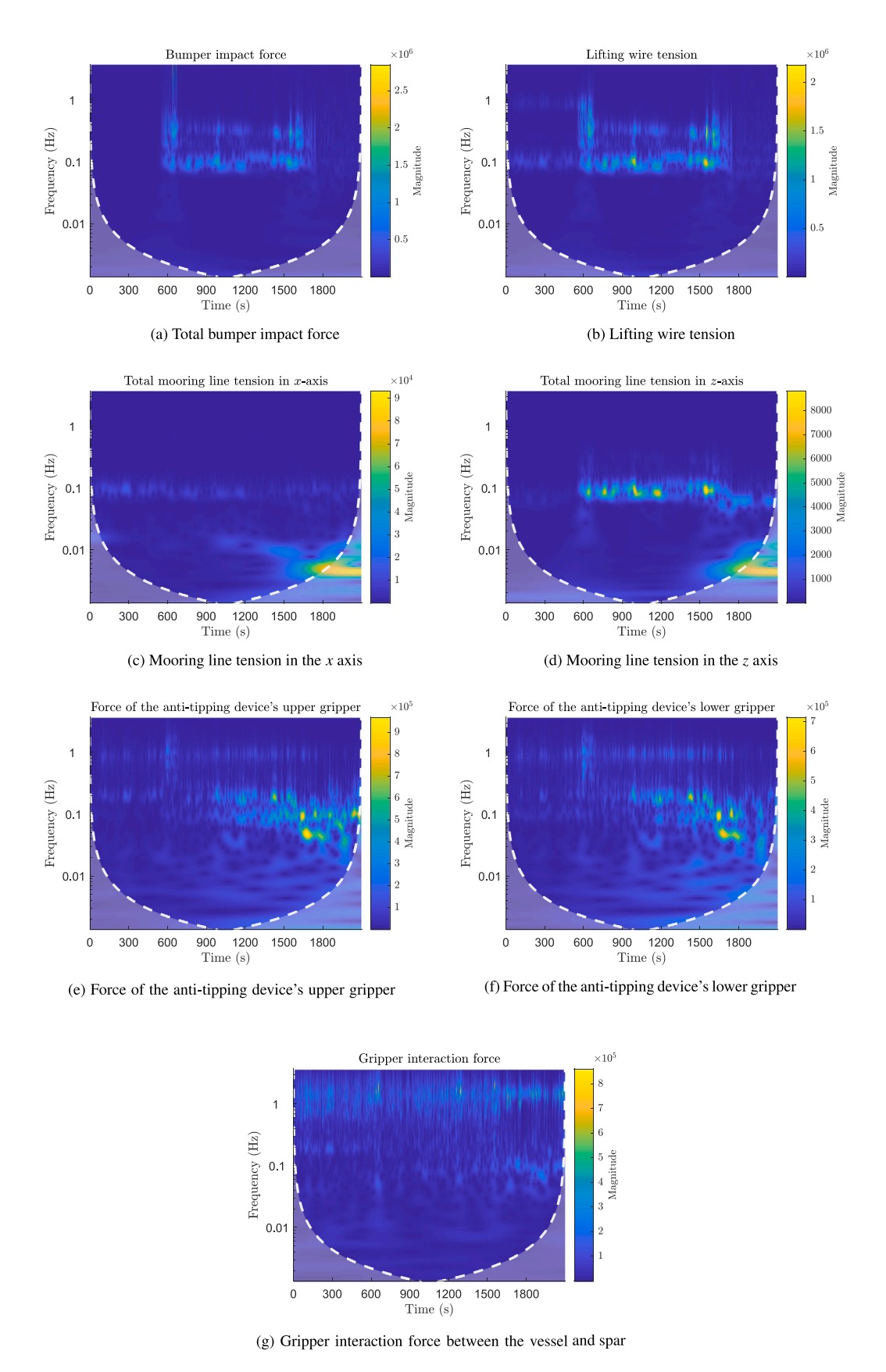
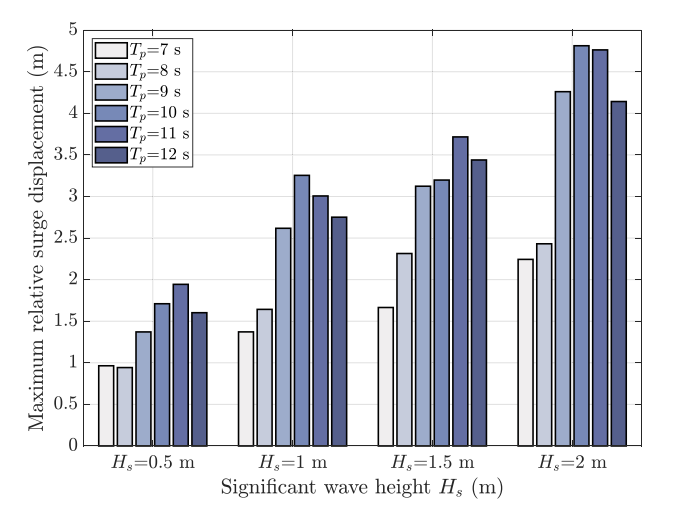
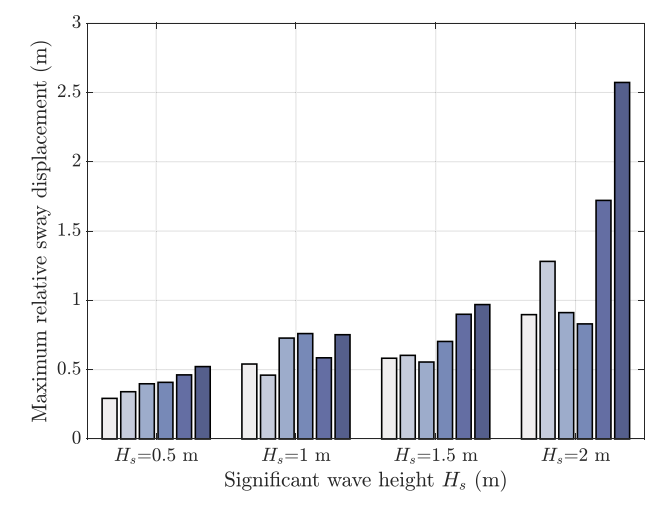


Fig. 15. Time-frequency analysis of coupling forces in WS1.





(a) Maximum relative surge displacement

(b) Maximum relative sway displacement

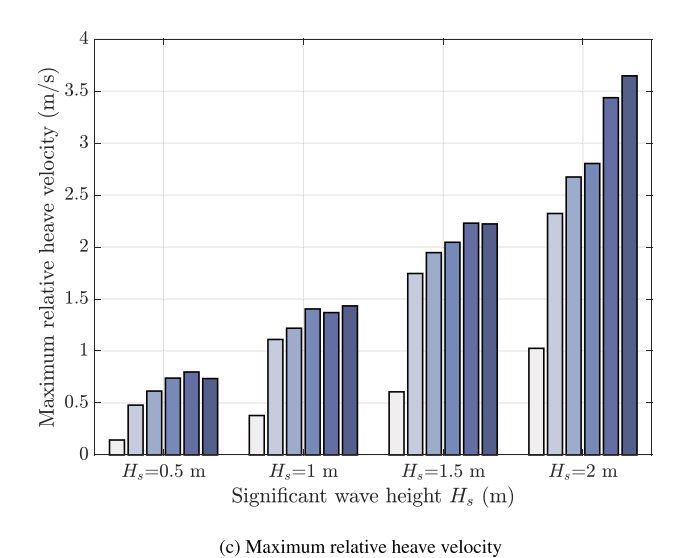


Fig. 16. Maximum relative motion in different sea states.

the vessel's pitch motion, the heave velocities of both the vessel and the spar, and the lowering speed. Besides, the magnitude of the forces exerted by the mechanical gripper and the anti-tipping device does not significantly change with variations in winch speed. During the process of payload lowering, jerks in the lifting wire tension become more pronounced. The jerks in dynamic tension increase the risk of losing control during the lowering operation, potentially causing component overload and leading to mechanical failure or system malfunction.

Fig. 15 presents the time–frequency analysis of the coupling forces in WS1. During the lowering operation phase, after the lifted assembly makes contact with the spar, both the bumper impact and lifting wire tension exhibit higher frequency components in addition to peak wave frequency. When the lowering operation is accomplished, the winch stops. The mooring line tensions correspond to the surge displacement, generating low-frequency components. Similarly, low-frequency components are generated in the anti-tipping forces and the vessel-spar gripper force. The high-frequency components around 1 Hz in the lifting wire tension, anti-tipping forces, and the vessel-spar gripper force may be attributed to the relatively high stiffness of the gripper and the lifting wires.

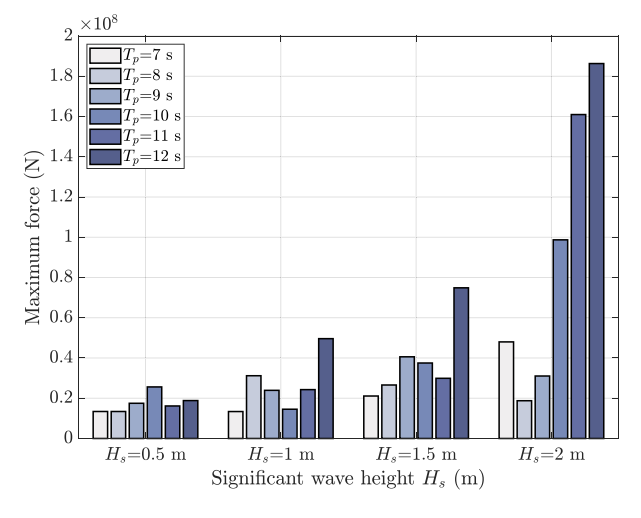
To sum up, the start time instant of the lowering operation and the winch speed setting determine the real-time sea state conditions during the operation, further influencing the re-impact and backward motion of the installation system. Excessive wire tension and impact forces can cause negative effects to both the wind turbine and the installation success rate. Thus, monitoring the key environmental parameters and motion states is necessary for the lowering operation.

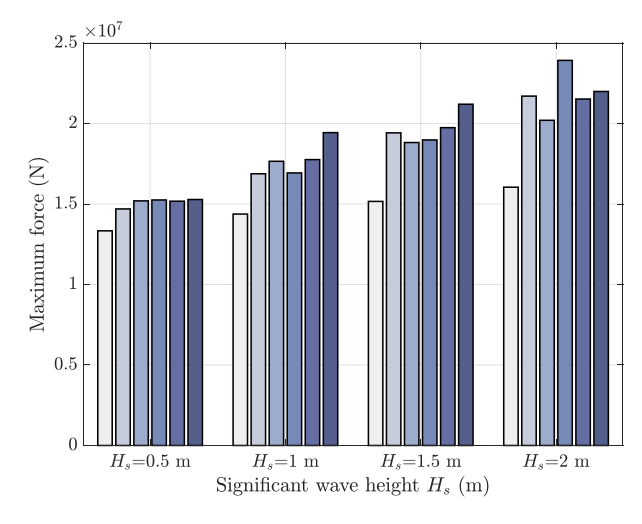
#### 4.4. Motion behavior in different sea states

Determining weather windows and performing tasks under allowable sea states are crucial for offshore operations. Simulations of the lowering operation are conducted under various environmental conditions, specific parameter settings are shown in Table 7.

Fig. 16 shows the maximum relative surge displacement, sway displacement, and heave velocity between the mating points during the lowering operation. The amplitude of relative surge displacement is higher than the relative sway displacement since the main wave direction coincides with the heading. At the same  $T_p$ , the amplitude

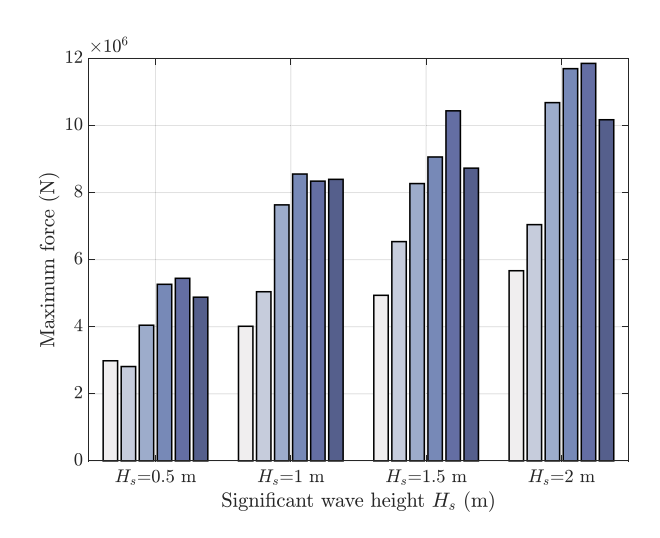
C. Ma et al. Renewable Energy 243 (2025) 122528

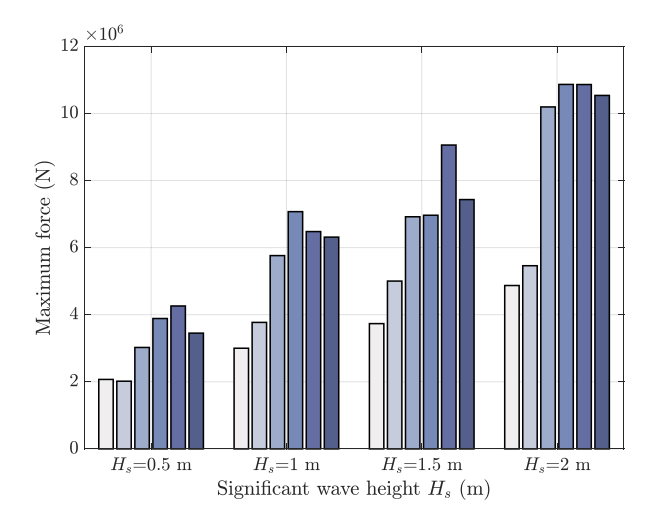




(a) Maximum total bumper impact forces

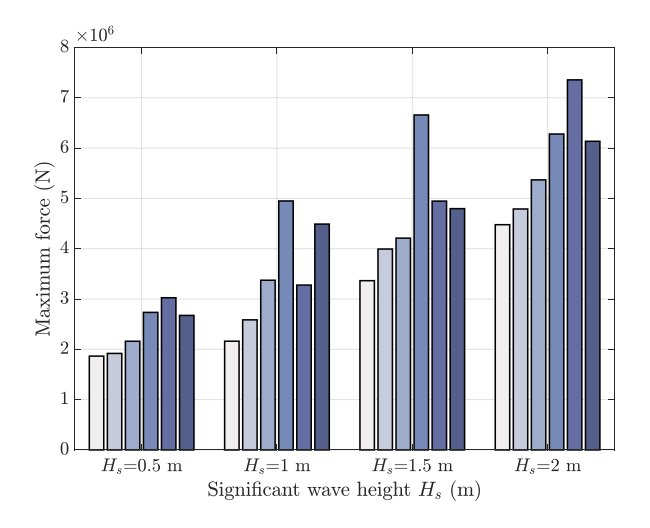






(c) Maximum forces of the upper gripper of the anti-tipping device

(d) Maximum forces of the lower gripper of the anti-tipping device



(e) Maximum gripper forces between the vessel and spar

 $\textbf{Fig. 17.} \ \ \text{Maximum coupling forces in different sea states}.$ 

Table 7
Sea states analyzed in the study.

EC	$H_s$ (m)	$T_p$ (s)	$U_w$ (m/s)	Lowering speed $v_l$ (m/s)
1	0.5	7,8,9,10,11,12	3	0.05
2	1	7,8,9,10,11,12	5	0.05
3	1.5	7,8,9,10,11,12	7	0.05
4	2	7,8,9,10,11,12	8	0.05

of the maximum relative motions grows as  $H_s$  increases. A 0.5 m increase in significant wave height leads to an average increase of 40.4% in maximum relative surge displacement, 53% in maximum sway displacement, and 71.4% in maximum heave velocity. At the same significant wave height  $H_s$ , the relative motions between mating points do not follow a simple linear relationship with  $T_p$ . When  $T_p$  of the wave spectrum approaches the system's natural periods, the installation system is induced to exhibit larger motion responses.

Fig. 17 shows the maximum coupling forces in different sea states. As the significant wave height  $H_{\scriptscriptstyle S}$  increases, greater wave forces are generated, resulting in a corresponding increase in the amplitude of each coupling force. A greater challenge is posed to the safety of mechanical devices and lifting lines. For bumper impact forces, their maximum values are approximately equal to the OWT gravity under lower sea states, i.e.,  $H_{\scriptscriptstyle S}=0.5$  m. However, the bumper impact forces exceed the gravity of the OWT as the  $H_{\scriptscriptstyle S}$  increases. Under higher sea states, the increased relative velocities between the OWT and spar generate huge impact forces. The maximum lifting wire tension arises from the sudden tightening of the wire. The intervals between re-impacts of the OWT and spar may widen in higher sea state, resulting in greater tension forces in lifting wire. The substantial impact forces could potentially damage the wind turbine structure and lead to operational failure, while jerks in dynamic tension pose similar hazards.

At the same  $H_s$ , the maximum forces of the grippers in the antitipping device vary with changes in  $T_p$ . The variation is associated with the motion responses of the vessel under different  $T_p$ . A larger motion response of the vessel necessitates greater gripper forces to restrict the tilt of the OWT. The trend of the maximum gripper force between the vessel and spar is similar to that of the maximum relative surge displacement. For a docking cone with linear stiffness, the maximum gripper force is proportional to the maximum relative displacement at the gripper location.

To sum up, the environmental loads significantly influence the dynamics of the installation system. In high sea states, the relative motion between mating points increases, exerting greater forces on mechanical components such as grippers and lifting wires. The increased forces can challenge the structural limits of the components, potentially compromising the success of the installation process. Therefore, it is essential to conduct a comprehensive structural limit assessment and operability analysis.

#### 5. Conclusions

This study considers the lowering operation of a tower–nacelle-rotor assembly using an integrated installation method. The dynamic response of the entire process is investigated through numerical simulations. The impact forces between the OWT and the spar during offshore installation operations are analyzed. The main conclusions are as follows:

- (1) During the lowering operation, heavy load transfer occurs, causing the installation vessel to tilt and move backward. An efficient DP control system can significantly reduce the backward motions. However, the propeller thrust and DP controller gains are limited and must be carefully calibrated before the operation.
- (2) After the initial impact, an incomplete load transfer to the spar leads to repeated separation-collision, i.e., re-impact phenomenon, threatening structural safety. The re-impact magnitude is primarily

determined by the relative speed between the spar and the payload, which is influenced by sea conditions, structures' motion responses, and lowering speed.

- (3) Increasing the winch speed can effectively reduce the duration of re-impacts. Due to the motion of the spar and vessel under irregular environmental loads, the start time instant of the lowering operation also influences the re-impact. Therefore, during the lowering operation, environment sensing and motion state monitoring are beneficial for decision-making.
- (4) Assessment of operability should focus on the coupling forces, which are significantly affected by sea conditions. In high sea states, it is essential to focus on the impact forces between the OWT and spar, as well as the sudden changes in the tension of the lifting wire.
- (5) The system dynamics of the novel T&I system and the lowering operation are complex. The selection of different lowering start instants within a short period can lead to significant variations in the dynamic process. As frequency-domain methods offer only limited insights, time-domain analysis is necessary for a more comprehensive understanding.

This research establishes a framework under unidirectional environmental loads due to the system's complexity. Future research could investigate the effects of multi-directional environmental loads on the installation system for a more comprehensive analysis. Additionally, the role of ballast water in adjusting system posture during installation requires further investigation to better understand its influence on the lowering operation. Since this study focuses on the overall system responses, the contact forces and impact processes require further study. Integrating finite element analysis for structural strength evaluation is also a potential area for future research.

#### CRediT authorship contribution statement

Can Ma: Writing – original draft, Visualization, Software, Methodology. Taiyu Zhang: Writing – review & editing. Zhiyu Jiang: Writing – review & editing. Zhengru Ren: Writing – review & editing, Methodology, Funding acquisition.

#### **Declaration of competing interest**

The authors declare that they have no known competing financial interests or personal relationships that could have appeared to influence the work reported in this paper.

#### Acknowledgments

This work was supported by Shenzhen Science and Technology Program (KJZD20231023100459001, JCYJ20240813112006009) and Natural Science Foundation of Guangdong Province, China (Grant No. 2024A1515011731).

#### References

- [1] J. Fu, W. Shi, X. Han, M. Karimirad, T. Wang, X. Li, Development and performance study of a multi-degree-of-freedom loading device for real-time hybrid model testing of floating offshore wind turbines, Mar. Struct. 99 (2025) 103717.
- [2] B. Wen, Z. Liang, H. Zhang, K. Fan, Y. Wang, D. Li, X. Tian, Z. Peng, A multi-drive aerodynamic load simulator for floating wind turbine model tests: Development, test and application, Ocean Eng. 286 (2023) 115579.
- [3] S. Wang, T. Moan, Z. Gao, Time-Domain Fatigue Analysis Methodology for Semi-Submersible Hulls of Floating Wind Turbines, Available at SSRN 5080108.
- [4] B.R. Sarker, T.I. Faiz, Minimizing transportation and installation costs for turbines in offshore wind farms, Renew. Energy 101 (2017) 667–679.
- [5] J. Lian, F. Ye, P. Wang, Y. Guo, H. Wang, T. Xiao, D. Xiong, Integrated transportation of offshore wind turbine and bucket foundation based on a U and K shaped assembled platform, Ocean Eng. 275 (2023) 114096.
- [6] W. Guachamin Acero, Z. Gao, T. Moan, Numerical study of a novel procedure for installing the tower and rotor nacelle assembly of offshore wind turbines based on the inverted pendulum principle, J. Mar. Sci. Appl. 16 (2017) 243–260.

- [7] M. Hassan, C. Guedes Soares, Dynamic analysis of a novel installation method of floating spar wind turbines, J. Mar. Sci. Eng. 11 (7) (2023).
- [8] Windfarm installation vessel, 2021, https://www.huismanequipment.com/en/ products/renewables/offshore\_wind/windfarm-installation-vessel.
- [9] K.H. Halse, S. Hong, B. Ataei, T. Liu, S. Yuan, H.P. Hildre, Design of floating installation vessel for offshore installation of floating offshore wind turbines, in: International Marine Design Conference, 2024.
- [10] Windspider, 2023, https://windspider.com/products/.
- [11] Y. Zhao, Z. Cheng, Z. Gao, P.C. Sandvik, T. Moan, Numerical study on the feasibility of offshore single blade installation by floating crane vessels, Mar. Struct. 64 (2019) 442–462.
- [12] Z. Jiang, L. Li, Z. Gao, K.H. Halse, P.C. Sandvik, Dynamic response analysis of a catamaran installation vessel during the positioning of a wind turbine assembly onto a spar foundation, Mar. Struct. 61 (2018) 1–24.
- [13] B. Koo, A. Magee, K. Lambrakos, E. Beyko, A. Sablok, Prediction of motions and loads for floatover installation of spar topsides, in: International Conference on Offshore Mechanics and Arctic Engineering, Vol. 49095, 2010, pp. 373–386.
- [14] S. Hong, H. Zhang, T.S. Nord, K.H. Halse, Effect of fender system on the dynamic response of onsite installation of floating offshore wind turbines, Ocean Eng. 259 (2022).
- [15] R. Skjetne, Z. Ren, A survey on modeling and control of thruster-assisted position mooring systems, Mar. Struct. 74 (2020) 102830.
- [16] B. Wang, X. Guo, X. Li, Wave feedforward control for dynamic positioning vessel under swell-dominated floatover condition: A numerical and experimental study, Appl. Ocean Res. 154 (2025) 104396.
- [17] B. Ataei, S. Yuan, Z. Ren, K.H. Halse, Effects of structural flexibility on the dynamic responses of low-height lifting mechanism for offshore wind turbine installation, Mar. Struct. 89 (2023) 103399.
- [18] Z. Ren, A.S. Verma, B. Ataei, K.H. Halse, H.P. Hildre, Model-free anti-swing control of complex-shaped payload with offshore floating cranes and a large number of lift wires, Ocean Eng. 228 (2021) 108868.
- [19] Z. Ren, R. Skjetne, A.S. Verma, Z. Jiang, Z. Gao, K.H. Halse, Active heave compensation of floating wind turbine installation using a catamaran construction vessel, Mar. Struct. 75 (2021) 102868.
- [20] P. Atzampou, P.C. Meijers, A. Tsouvalas, A.V. Metrikine, Contactless control of suspended loads for offshore installations: Proof of concept using magnetic interaction, J. Sound Vib. 575 (2024) 118246.
- [21] T. Liu, K.H. Halse, B.J. Leira, Z. Jiang, W. Chai, H.-P. Brathaug, H.P. Hildre, Dynamic response of a SWATH vessel for installing pre-assembled floating wind turbines, Mar. Struct. 88 (2023).
- [22] S. Hong, H. Zhang, K.H. Halse, Hydrodynamic and environmental modelling influence on numerical analysis of an innovative installation method for floating wind, Ocean Eng. 280 (2023) 114681.
- [23] J. Liu, Z. Xiao, K. Wang, S. Huang, Y. Du, Comparative study on dynamic responses of integrated installation process of a 5-MW and a 15-MW offshore wind turbine considering a pre-installed foundation, Ocean Eng. 299 (2024) 117399.
- [24] D.F. Domingos, P. Wellens, J.-W. van Wingerden, Frequency-domain framework for floating installation of wind-turbine towers. Ocean Eng. 297 (2024) 116952.
- [25] B. Li, D. Qiao, W. Zhao, Z. Hu, S. Li, Operability analysis of SWATH as a service vessel for offshore wind turbine in the southeastern coast of China, Ocean Eng. 251 (2022) 111017.
- [26] L. Li, Z. Gao, T. Moan, Operability analysis of monopile lowering operation using different numerical approaches, Int. J. Offshore Polar Eng. 26 (02) (2016) 88–99.
- [27] B. Ataei, Z. Ren, K.H. Halse, Design of a quick-connection device for installing pre-assembled offshore wind turbines, Mar. Struct. 100 (2025) 103720.
- [28] A.S. Verma, N.P. Vedvik, Z. Gao, A comprehensive numerical investigation of the impact behaviour of an offshore wind turbine blade due to impact loads during installation, Ocean Eng. 172 (2019) 127–145.
- [29] Y. Guo, M. Alam, Nonlinear bending and thermal postbuckling of magnetoelectro-elastic nonlocal strain-gradient beam including surface effects, Appl. Math. Model. (2025) 115955.

- [30] M. Alam, Y. Guo, Y. Bai, S. Luo, Post-critical nonlinear vibration of nonlocal strain gradient beam involving surface energy effects, J. Sound Vib. (2025) 118930.
- [31] K. Ellermann, E. Kreuzer, Nonlinear dynamics in the motion of floating cranes, Multibody Syst. Dyn. 9 (2003) 377–387.
- [32] O. Makarov, T. Harada, Parametric sensitivity of crane ship numerical model with experimental verification in a wave basin, Ocean Eng. 286 (2023) 115554.
- [33] N. Ku, M.-I. Roh, Dynamic response simulation of an offshore wind turbine suspended by a floating crane, Ships Offshore Struct. 10 (6) (2015) 621–634.
- [34] B. Rong, X. Rui, K. Lu, L. Tao, G. Wang, F. Yang, Dynamics analysis and wave compensation control design of ships seaborne supply by discrete time transfer matrix method of multibody system, Mech. Syst. Signal Process. 128 (2019) 50-68
- [35] N. Ullah, M. Duan, A. Syed, M. Sajid, G. Sun, W. Li, et al., Multibody constrained dynamics of deepwater Y-method installation system, Ocean Eng. 278 (2023) 114482
- [36] A.F. Haselsteiner, J.-H. Ohlendorf, S. Oelker, L. Ströer, K.-D. Thoben, K. Wiedemann, E. De Ridder, S. Lehmann, Lifting wind turbine components from a floating vessel: A review on current solutions and open problems, J. Offshore Mech. Arct. Eng. 141 (5) (2019) 050801.
- [37] J.-H. Cha, M.-I. Roh, K.-Y. Lee, Dynamic response simulation of a heavy cargo suspended by a floating crane based on multibody system dynamics, Ocean Eng. 37 (14–15) (2010) 1273–1291.
- [38] K.-P. Park, J.-H. Cha, K.-Y. Lee, Dynamic factor analysis considering elastic boom effects in heavy lifting operations, Ocean Eng. 38 (10) (2011) 1100–1113.
- [39] L. Li, Z. Gao, T. Moan, H. Ormberg, Analysis of lifting operation of a monopile for an offshore wind turbine considering vessel shielding effects, Mar. Struct. 39 (2014) 287–314.
- [40] C. Ma, Z.-Z. Hu, X.Y. Zheng, Z. Ren, Inertia load reduction for loadoff during floating offshore wind turbine installation: Release decision and ballast control, Sustain. Horizons 10 (2024) 100096.
- [41] T. Zhang, Z. Ren, Restricted isometry property in wave buoy analogy and application to multispectral fusion, IEEE Trans. Intell. Transp. Syst. (2025).
- [42] M. Burhan, Q. Chen, M.W. Shahzad, D. Ybyraiymkul, F.H. Akhtar, K.C. Ng, Innovative concentrated photovoltaic thermal (CPV/T) system with combined hydrogen and MgO based storage, Int. J. Hydrog. Energy 46 (31) (2021) 16534–16545.
- [43] Y. Chen, Y. Ding, Z.-Z. Hu, Z. Ren, Geometrized task scheduling and adaptive resource allocation for large-scale edge computing in smart cities, IEEE Internet Things J. (2025).
- [44] J. Zheng, P. Liang, H. Zhao, W. Deng, A broad sparse fine-grained image classification model based on dictionary selection strategy, IEEE Trans. Reliab. (2023)
- [45] P. Wang, X. Tian, T. Peng, Y. Luo, A review of the state-of-the-art developments in the field monitoring of offshore structures, Ocean Eng. 147 (2018) 148–164.
- [46] M. van Beek, A feasibility study for the installation of 10 MW offshore wind turbines with an SSCV, 2018.
- [47] M. Zou, M. Chen, L. Zhu, L. Li, W. Zhao, A constant parameter time domain model for dynamic modelling of multi-body system with strong hydrodynamic interactions, Ocean Eng. 268 (2023) 113376.
- [48] W. Zhao, J. Yang, Z. Hu, L. Tao, Prediction of hydrodynamic performance of an FLNG system in side-by-side offloading operation, J. Fluids Struct. 46 (2014) 89–110.
- [49] P. Cai, I. Chandrasekaran, J. Zheng, Y. Cai, Automatic path planning for dualcrane lifting in complex environments using a prioritized multiobjective PGA, IEEE Trans. Ind. Inform. 14 (3) (2018) 829–845.
- [50] H. Taghaddos, U. Hermann, A. Abbasi, Automated crane planning and optimization for modular construction, Autom. Constr. 95 (2018) 219–232.